

Supporting information

Precise control of TiO₂ overlayer on hematite nanorod arrays by ALD for the photoelectrochemical water splitting

Jiao Wang, Letizia Liccardo, Heydar Habibimarkani, Ewa Wierzbicka, Thorsten Schultz, Norbert Koch, Elisa Moretti, and Nicola Pinna**

Jiao Wang, Nicola Pinna

Department of Chemistry and the Center for the Science of Materials Berlin, Brook-Taylor-Str. 2, 12489 Berlin, Germany
E-mail: nicola.pinna@hu-berlin.de

Letizia Liccardo, Heydar Habibimarkani, Elisa Moretti

Department of Molecular Sciences and Nanosystems, Ca' Foscari University of Venice, Via Torino 155, 30172 Venezia Mestre, Italy
Email: elisa.moretti@unive.it

Ewa Wierzbicka

Department of Functional Materials and Hydrogen Technology, Faculty of Advanced Technologies and Chemistry, Military University of Technology, 2 Kaliskiego Street, Warsaw 00908, Poland

Thorsten Schultz, Norbert Koch

Institut für Physik and IRIS Adlershof, Humboldt-Universität zu Berlin, Brook-Taylor-Str. 6, 12489 Berlin, Germany

Thorsten Schultz, Norbert Koch

Helmholtz-Zentrum Berlin für Materialien und Energie GmbH, Hahn-Meitner-Platz 1, 14109 Berlin, Germany

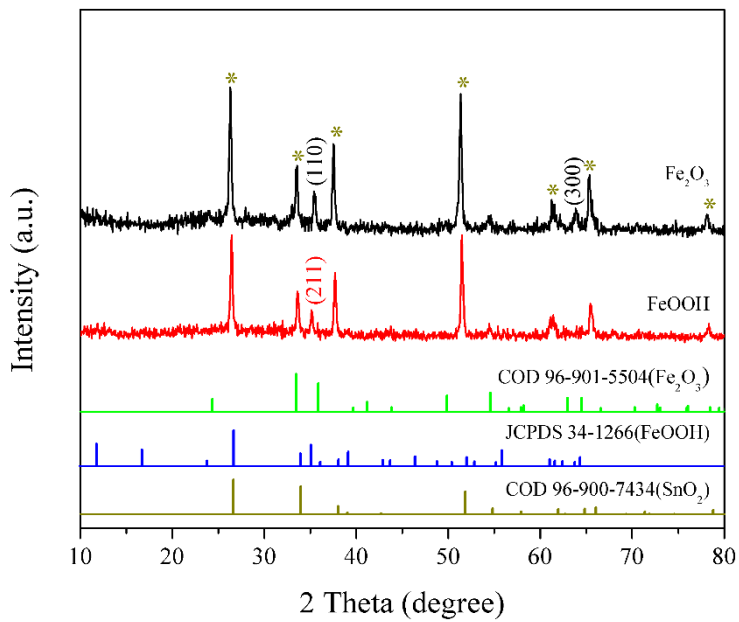


Figure S1. XRD patterns of pristine β -FeOOH and α -Fe₂O₃.

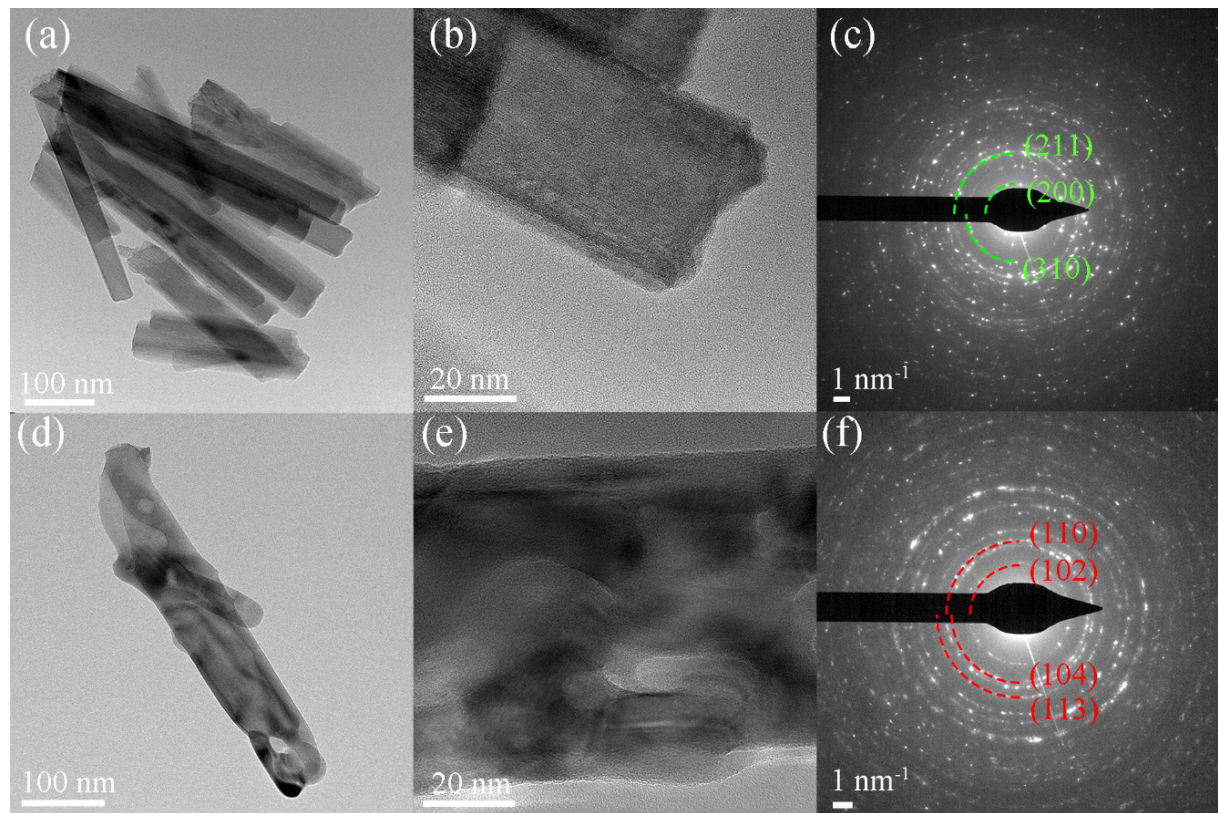


Figure S2. (a,b) TEM images of β -FeOOH nanorods. (c) Corresponding SAED pattern of β -FeOOH nanorods. (d,e) HRTEM images of α -Fe₂O₃ nanorods. (f) Corresponding SAED pattern of α -Fe₂O₃ nanorods.

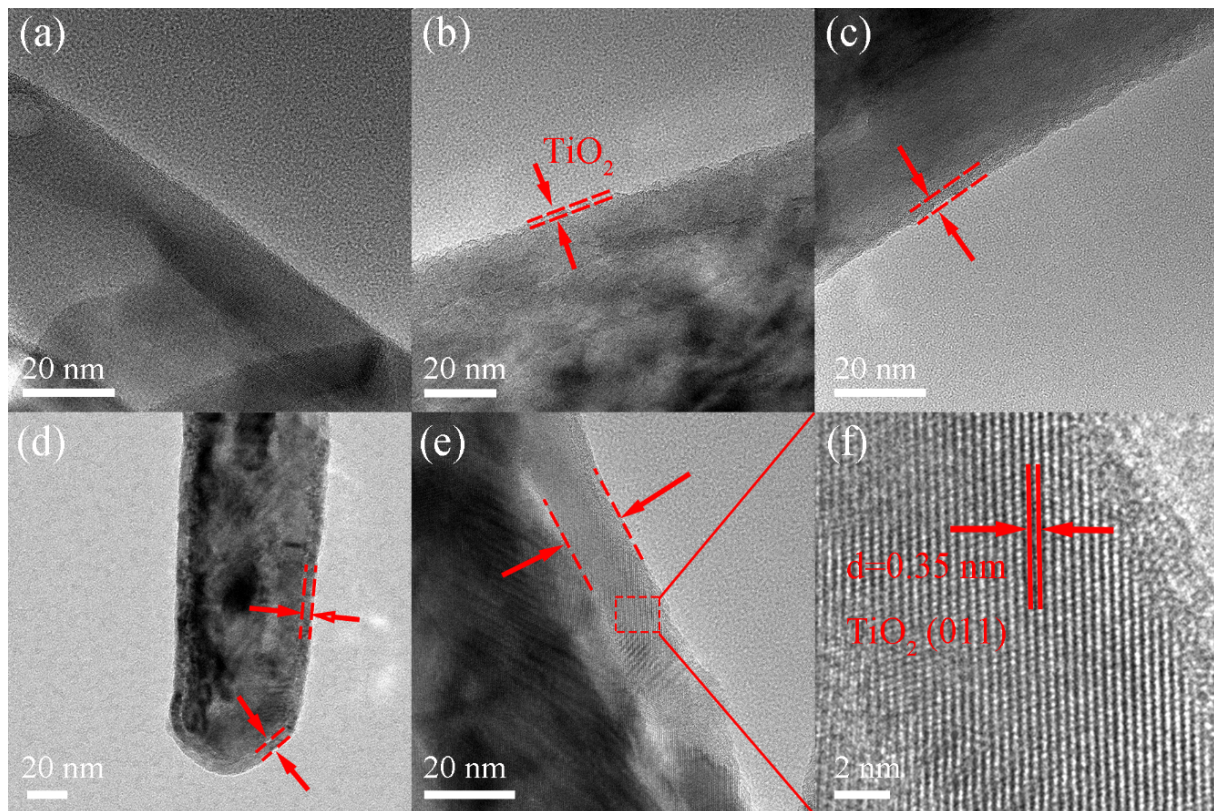


Figure S3. HRTEM images of TiO_2 deposited on pristine hematite with different ALD cycles: (a) TiO_2 -10/ Fe_2O_3 , (b) TiO_2 -20/ Fe_2O_3 , (c) TiO_2 -40/ Fe_2O_3 , (d) TiO_2 -80/ Fe_2O_3 , (e) TiO_2 -150/ Fe_2O_3 , (f) The magnified view of the lattice fringes of TiO_2 -150/ Fe_2O_3 .

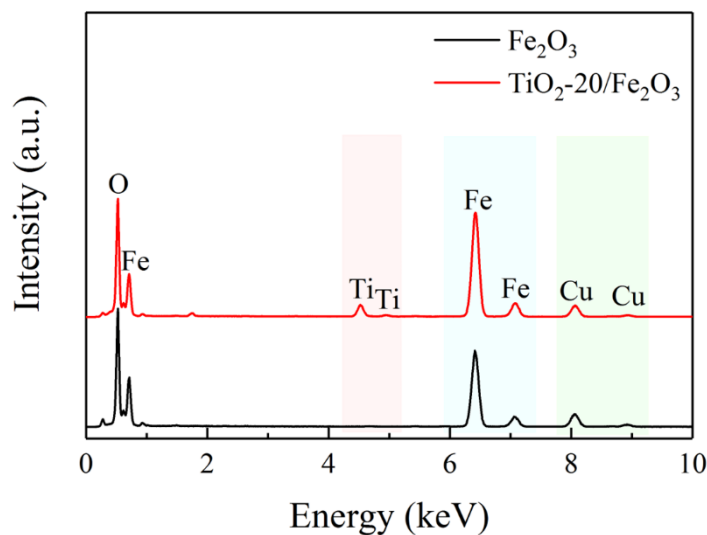


Figure S4. EDX spectra for pristine Fe_2O_3 and TiO_2 -20/ Fe_2O_3 analyzed on a copper TEM grid.

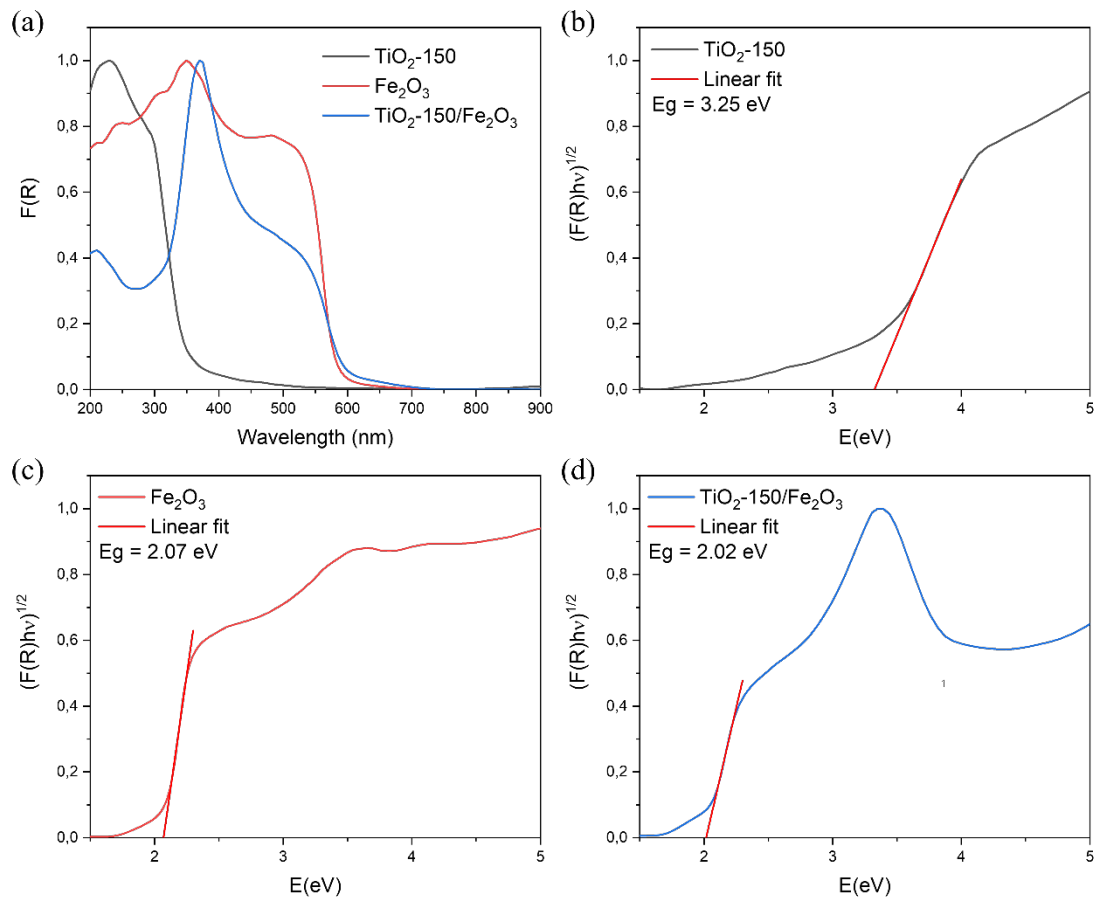


Figure S5. (a) Plots of $F(R)$ versus wavelength of the pristine Fe_2O_3 , pristine TiO_2 and $\text{TiO}_2/\text{Fe}_2\text{O}_3$ nanocomposites from the UV-vis diffuse reflectance spectra. Plots of $(F(R)\hbar\nu)^{1/2}$ versus photon energy for the (b) pristine TiO_2 (c) pristine Fe_2O_3 and (d) $\text{TiO}_2/\text{Fe}_2\text{O}_3$ heterojunction.

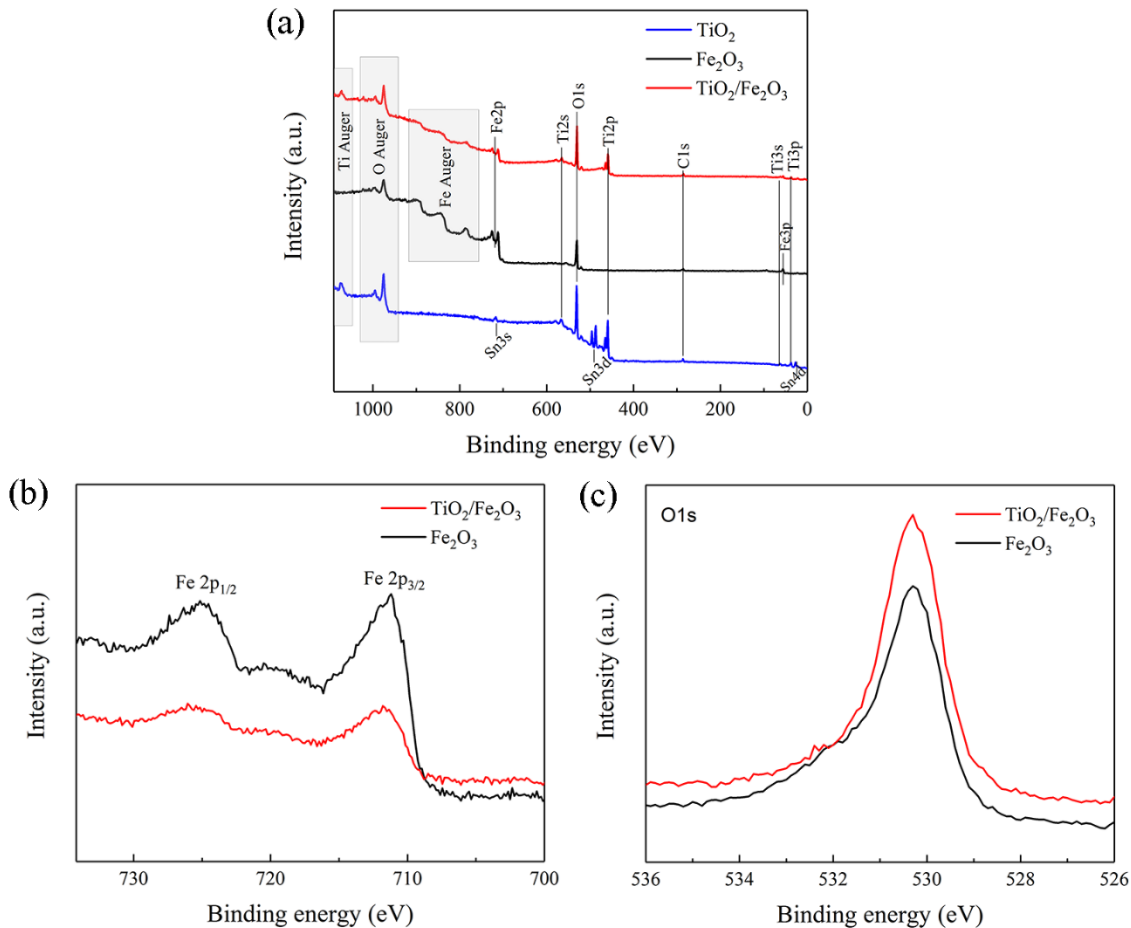


Figure S6. (a) XPS survey spectra of the pristine Fe_2O_3 , pristine TiO_2 with 20ALD cycles and Fe_2O_3 coated with 20 ALD cycles of TiO_2 overlayer. For the TiO_2 sample, the tin signal from the FTO substrate is visible due to the small thickness of the TiO_2 layer. (b) High-resolution $\text{Fe}2p$ photoelectron spectrum of the pristine Fe_2O_3 and TiO_2 -20/ Fe_2O_3 . (c) High-resolution $\text{O}1s$ photoelectron spectrum of pristine Fe_2O_3 and TiO_2 -20/ Fe_2O_3 .

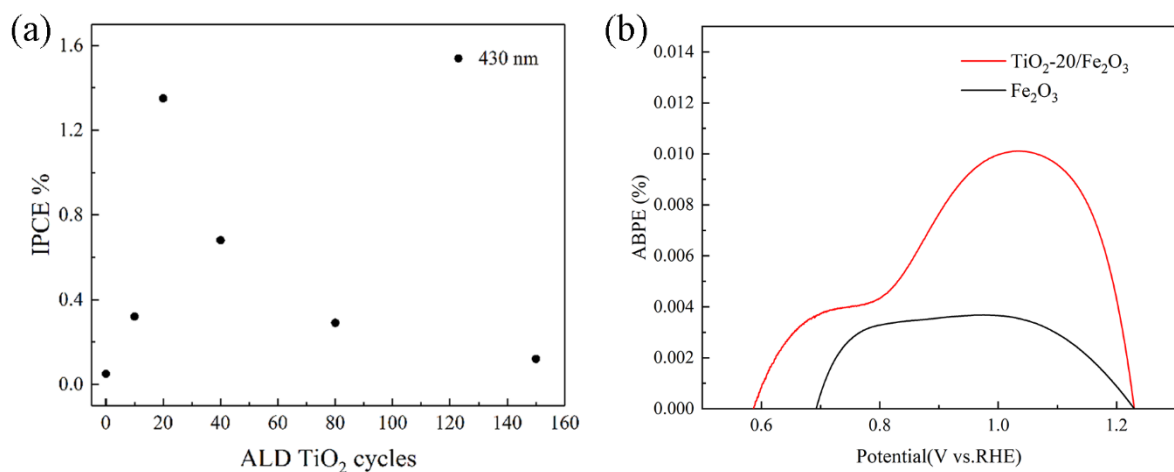


Figure S7. (a) IPCE spectra of pristine Fe_2O_3 and $\text{TiO}_2/\text{Fe}_2\text{O}_3$ photoanodes measured in 1M KOH at 0.5 V bias vs. Hg/HgO under 430 nm light irradiation. (b) ABPE of pristine Fe_2O_3 and TiO_2 -20/ Fe_2O_3 photoanodes.

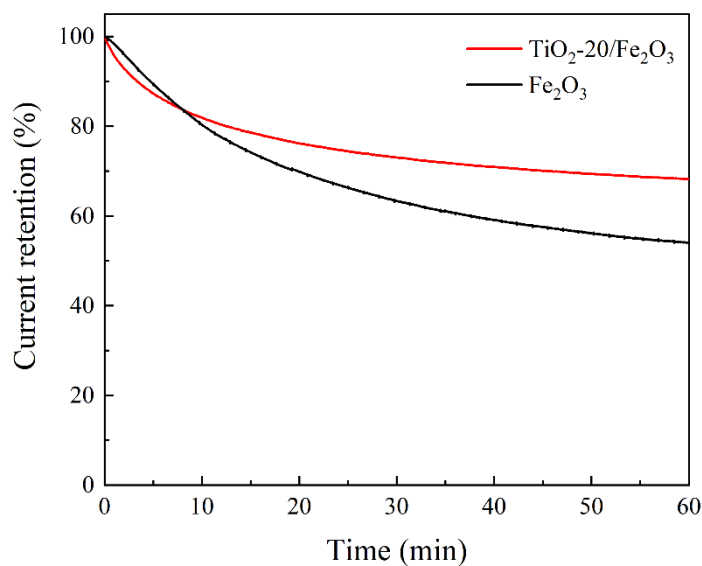


Figure S8. Stability test of pristine Fe_2O_3 and $\text{TiO}_2\text{-}20/\text{Fe}_2\text{O}_3$ photoanodes.

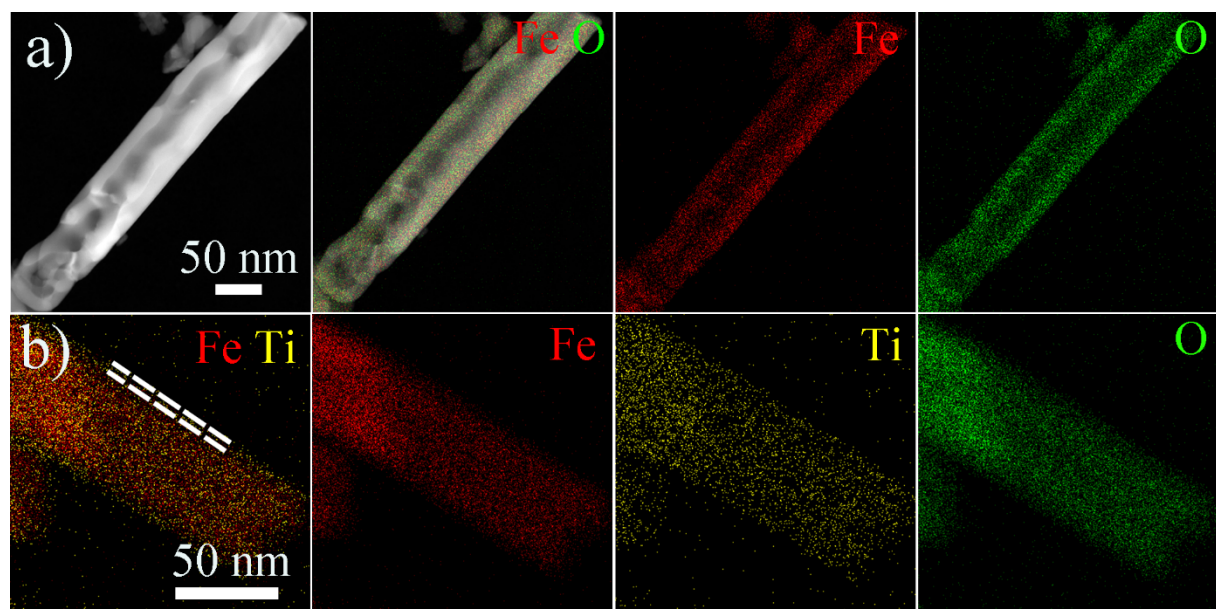


Figure S9. The morphology of the synthesized photocatalyst after stability test: a) pristine Fe_2O_3 , b) $\text{TiO}_2\text{-}20/\text{Fe}_2\text{O}_3$.

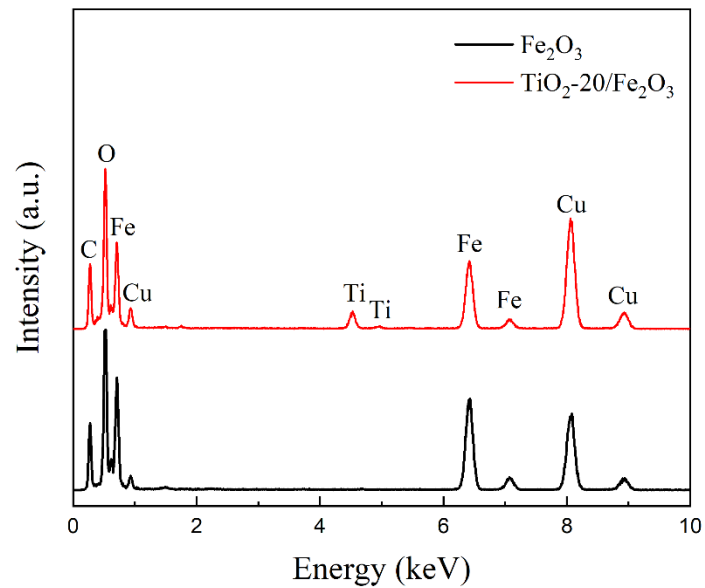


Figure S10. The composition of the pristine Fe_2O_3 and $\text{TiO}_2\text{-}20/\text{Fe}_2\text{O}_3$ after stability test.

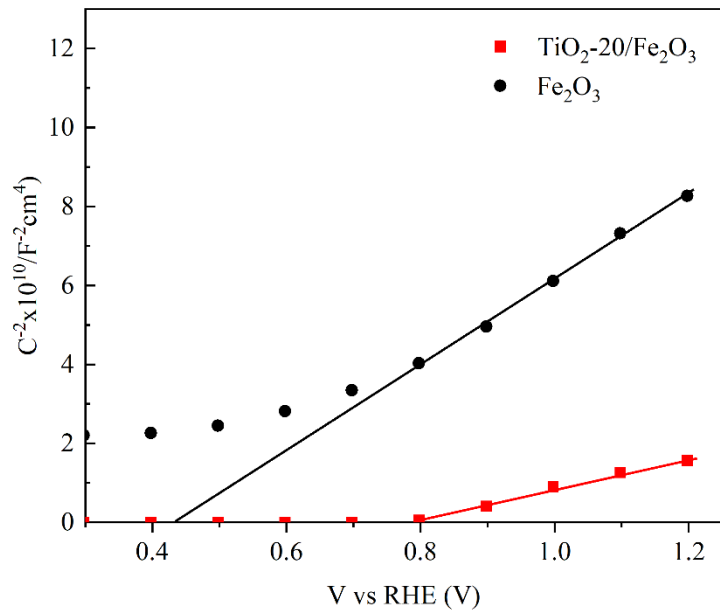


Figure S11. Mott-Schottky plots of pristine Fe_2O_3 and $\text{TiO}_2\text{-}20/\text{Fe}_2\text{O}_3$ heterostructure.

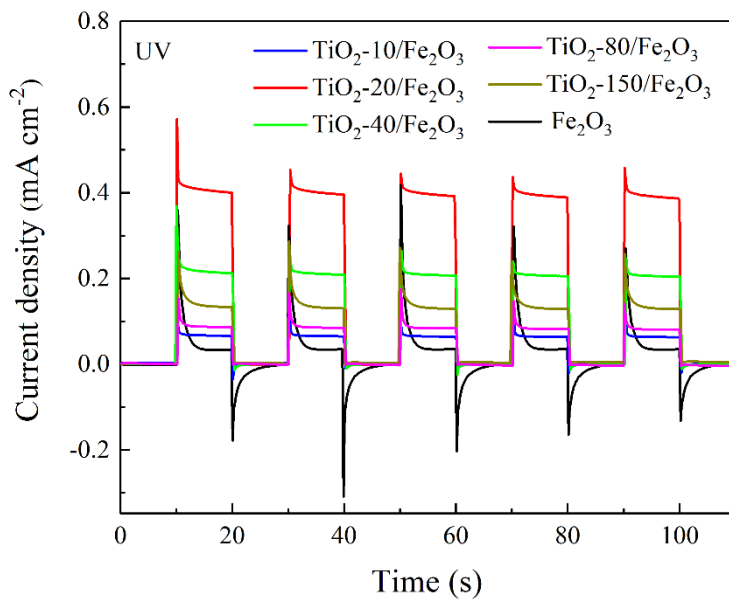


Figure S12. Time-based photocurrent density for pristine and TiO_2 -coated hematite photoanodes at 0.5 V bias vs. Hg/HgO under UV light irradiation.

Table S1. Average TiO_2 overlayer thickness and the GPC calculated from TEM micrographs and spectroscopic ellipsometry.

Samples	Transmission electron microscopy		Spectroscopic ellipsometry	
	Thickness (nm)	Slope of line fit (GPC)	Thickness (nm)	Slope of line fit (GPC)
$\text{TiO}_2\text{-}10/\text{Fe}_2\text{O}_3$	---		2.2	
$\text{TiO}_2\text{-}20/\text{Fe}_2\text{O}_3$	1.7		3.5	
$\text{TiO}_2\text{-}40/\text{Fe}_2\text{O}_3$	3.5	0.88 Å	5.0	0.96 Å
$\text{TiO}_2\text{-}80/\text{Fe}_2\text{O}_3$	6.8		9.0	
$\text{TiO}_2\text{-}150/\text{Fe}_2\text{O}_3$	13.2		15.1	

Table S2. The atomic/weight percentage of all the samples with different ALD cycles.

Samples	Atom fraction (%)		Mass fraction (%)	
	Ti	Fe	Ti	Fe
$\text{TiO}_2\text{-}10/\text{Fe}_2\text{O}_3$	1.28	28.2	2.21	57.0
$\text{TiO}_2\text{-}20/\text{Fe}_2\text{O}_3$	3.89	39.9	5.62	67.2
$\text{TiO}_2\text{-}40/\text{Fe}_2\text{O}_3$	6.59	24.7	11.3	49.3
$\text{TiO}_2\text{-}80/\text{Fe}_2\text{O}_3$	9.88	22.1	16.9	44.1
$\text{TiO}_2\text{-}150/\text{Fe}_2\text{O}_3$	18.4	22.7	28.5	41.0